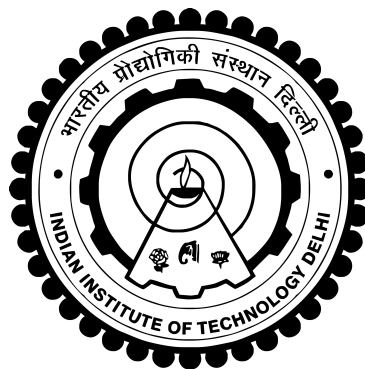


**INVESTIGATION ON LIGHT SCATTERING FROM
TURBID MEDIA THROUGH EXPERIMENTS AND
MONTE CARLO SIMULATIONS**

KALPAK GUPTA



**DEPARTMENT OF PHYSICS
INDIAN INSTITUTE OF TECHNOLOGY DELHI
APRIL 2022**

©Indian Institute of Technology Delhi (IITD), New Delhi, 2022

**INVESTIGATION ON LIGHT SCATTERING FROM
TURBID MEDIA THROUGH EXPERIMENTS AND
MONTE CARLO SIMULATIONS**

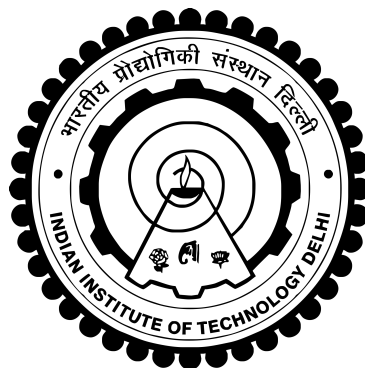
by

KALPAK GUPTA

Department of Physics

Submitted

*in fulfillment of the requirements of the degree of **Doctor of Philosophy**
to the*



INDIAN INSTITUTE OF TECHNOLOGY DELHI

APRIL 2022

Dedicated to my parents

Certificate

This is to certify that the thesis titled “**Investigation on light scattering from turbid media through experiments and Monte Carlo simulations**”, being submitted by **Kalpak Gupta** to the Indian Institute of Technology Delhi, for the award of the degree of **Doctor of Philosophy**, is a record of bonafide research work carried out by him. He has worked under my guidance and supervision and has fulfilled the requirements, which to my knowledge, have reached the requisite standard for the submission of this thesis. The results contained in this thesis have not been submitted in part or full to any other University or Institute for the award of any degree or diploma.

Date:

Place: New Delhi

Prof. M. R. Shenoy
Department of Physics
Indian Institute of Technology Delhi
New Delhi – 110016, India

Acknowledgements

First and foremost, I would like to express my deepest gratitude to my supervisor Prof. M. R. Shenoy for providing me the opportunity to work on the very fascinating field of light scattering and its applications. His ardent encouragement and support throughout the tenure of my Ph.D. enabled me to reify and explore my research problems from different perspectives, succoured by his vast experience, innovative ideas, and impeccable passion for research, which immensely helped in improving my knowledge and skills. I consider myself most fortunate to have worked under the kind guidance of Prof. Shenoy, who always gave me an affable milieu along with the freedom to work in my own style, while at the same time felicitously steering me towards my objectives whenever I required a boost of motivation. His unrelenting patience and positivity allayed much of the consternations one usually faces in a journey such as this, which has made him a source of inspiration I will cherish throughout my life.

I also give my sincere thanks to my SRC members, Prof. D. S. Mehta, Prof. Bhaskar Kanseri and Prof. R. Elangovan; the faculty members of the Fiber Optics Group, Prof. K. Thyagarajan, Prof. Anurag Sharma, Prof. Arun Kumar, Prof. B. D. Gupta and Prof. Ajit Kumar; and all the faculties of the Physics Department for providing me with their valuable insights and constructive suggestions during my Ph.D. tenure.

Though it is difficult to mention the name of all the individuals who contributed directly or indirectly towards this achievement, I would like to thank my seniors and colleagues at the Fiber Optics Group—Dr. Dinesh Sharma, Dr. Manoj Kumar, Dr. Ajanta Barh, Dr. Rana Tabassum, Dr. Divya Bharadwaj, Dr. Anand Mohan, Dr. Ranjeet Dwivedi, Dr. Parvinder Kaur, Dr. Deepa Chaturvedi Pandey, Dr. Pragati Aashna, Dr. Nabarun Saha, Dr. Jitender, Dr. Ramesh Kumar, Dr. Sugeet Sunder, Dr. Babita Bakshi (nee Kumari), Dr. Sruthi Prasood Usha, Dr. Ravi Kant, Dr. Vivek Semwal, Dr. Anisha Pathak, Nithin, Vikas, Subhajit, Priyadarshini, Ajay, Sukhvinder, Pratiksha, Anjali and Jully—as well as my seniors and friends from other research groups of IIT Delhi—Dr. Soumik Adhikary, Dr. Swagato Sarkar, Dr. Shashank Gahlaut, Dr. Mayank Gupta, Dr. Atul Kumar Dubey, Dr. Sethuraj R., Shahrukh Salim, Rajni, Gayatri, Hemant, Sunaina,

Mansi, and Deepika—for the enriching discussions and light hearted moments which obviated the sporadic ennui during the strenuous periods of work during the last few years.

I would like to acknowledge Mr. Vijay Kumar for his technical help and thank him for providing me with the various components of my experiments in the lab. I am also thankful to University Grants Commission (UGC), India for providing financial support through the award of JRF/SRF during the tenure of my Ph.D.

Lastly and most importantly, I am extremely thankful and grateful to my parents, Mr. Amitava Gupta and Mrs. Indrani Gupta, for their unwavering moral support and gracious blessings throughout the duration of my Ph.D.

Finally, I pay my humble obeisance to the almighty, without whose mercy this work would never have been possible.

Kalpaka Gupta

Abstract

Over the last few decades, light scattering techniques have become ubiquitous in a variety of applications, such as characterization of biological tissues, detection and analysis of particles and sediments in water, including sea water, and monitoring of air pollution. When light interacts with matter, the phenomena of scattering and absorption occur, and the characteristics of the interaction depend on the physical properties of the scattering particle. The general aim of various light scattering methodologies is to use the measurement of scattered light to obtain information about such scattering particles, especially in the case of a turbid medium, which consists of suspended particles undergoing random motion inside it.

A turbid medium is characterized by scattering parameters—such as the interaction coefficient μ_t and the anisotropy parameter g —which describe the propagation of light inside the medium. μ_t is proportional to the concentration of particles, and determines the amount of extinction that light suffers while propagating through the medium, while g is a measure of the angular anisotropy of the scattered light. These scattering parameters depend on the properties of the scattering particles present in the medium, such as their shape, size, and concentration. Currently, there exists several methods to characterize a turbid medium, i.e., to determine the scattering parameters of the medium, from which various physical properties of the constituent particles can be obtained. However, most of the reported methods to characterize such media are either expensive or complex, which vary in accordance to the desired accuracy and robustness for a given application. In this thesis, we present our investigation on light scattering from turbid media using experimental measurements in conjunction with analytical and numerical calculations, with the aim of establishing methods which are relatively simpler, require fewer components, and are easier to implement.

Our methodologies involve the measurement of the scattered light from a turbid medium using appropriately placed photodetectors, and comparing the measured power with numerically obtained scattered power for different combinations of the scattering parameters. The simulations are performed by using the Monte Carlo method, and the scattering parameter(s)

for which the scattered power at the detector(s) match with the measured power are inferred to be the correct scattering parameter(s) of the given turbid medium. In our studies, we first apply the methodology to measure the scattered light from a given turbid medium at a detector, for determination of the anisotropy parameter g of the medium. In the proposed method, the interaction coefficient μ_t of a given sample is first determined from the measurement of the unscattered light by using the Beer-Lambert law; then the scattered power from the sample at an angle θ is measured using a photodetector. The g of the medium is estimated corresponding to the measured scattered power from a calibration curve relating the scattered power to g , which is obtained from Monte Carlo simulations. It is also discussed that the same methodology can be applied to obtain the particle size in the case of monodisperse turbid solutions comprising spherical particles. However, it is seen that there are two possible values of g (or particle size) corresponding to a single position of the detector. Subsequently, we show that by using two detectors placed at two different positions to measure the scattered power, the g or the particle size can be uniquely determined.

The estimation of μ_t requires the measurement of the undeviated transmitted light, for which the corresponding detector has to be placed far away (≈ 1 m) from the turbid sample. To reduce the bulk of the experimental setups due to this requirement, we also propose the use of a pair of parallel mirrors to multifold the transmitted beam from the given sample, to increase the effective path length of the beam. This makes it possible to estimate μ_t accurately by keeping the detector relatively close to the sample, leading to a compact setup. We further present a method to determine the size of microspheres in a turbid solution by using analytical calculations instead of simulations, with the restriction that the particles are concentrated within a very small region inside the sample. The method requires two detectors placed close to the sample, to measure the scattered power at two different positions; in the proposed scheme, the estimation of μ_t is not required at all, which again leads to a compact setup.

Studies on mixtures are performed as well, where a mixture refers to a turbid medium comprising different types of particles. From first principles, we arrive at a scheme to simulate light propagation in a mixture using the Monte Carlo model, and then apply it to determine the

concentrations of known type of constituents in a bidisperse mixture, by following a similar methodology of comparing the measured scattered power to the simulated power for different relative concentrations of the constituent particles. Finally, we make use of the Monte Carlo simulations to simulate the calibration curve relating the scattered power to the particle size or g for different operating wavelengths and detector positions, and show that our method can be optimized in terms of the dynamic range and sensitivity by appropriately choosing these physical factors in the experimental setup. We further show that the experimental setup can be implemented using optical fibers to transport light to/from the sample, which provides additional advantages like robustness, durability, and scope of telemetry for remote sensing applications.

सार

पिछले कुछ दशकों में, विभिन्न प्रकार के अनुप्रयोगों में प्रकाश प्रकीर्णन की तकनीक सर्वव्यापी हो गई है, जैसे कि जैविक ऊतकों का लक्षण वर्णन, समुद्र के पानी सहित पानी में कणों और तलछट का पता लगाना और विश्लेषण करना, और वायु प्रदूषण की निगरानी करना। जब प्रकाश पदार्थ के साथ अंतःक्रिया करता है, तो प्रकीर्णन और अवशोषण की घटनाएं होती हैं, और वह क्रिया की विशेषताएं बिखराने वाले कणों के भौतिक गुणों पर निर्भर करती हैं। विभिन्न प्रकाश प्रकीर्णन पद्धतियों का सामान्य उद्देश्य ऐसे प्रकीर्णन कणों के बारे में जानकारी प्राप्त करने के लिए प्रकीर्ण प्रकाश के माप का उपयोग करना है, विशेष रूप से एक पंकिल माध्यम के मामले में, जिसके अंदर यादृच्छिक गति से गुजरने वाले निलंबित कण होते हैं।

एक पंकिल माध्यम का प्रकीर्णन का मापदंडों की विशेषता होती है प्रकीर्णन प्राचल—जैसे अंतःक्रिया गुणांक μ_t और अनिसोट्रॉपी प्राचल g —जो उस माध्यम के अंदर प्रकाश के प्रचार का वर्णन करते हैं। μ_t कणों की सांद्रता के समानुपाती होता है, और माध्यम में प्रचार होता हुआ प्रकाश के विलुप्त होने की मात्रा को निर्धारित करता है, जबकि g प्रकीर्ण प्रकाश के कोणीय अनिसोट्रॉपी का एक मात्रा है। ये प्रकीर्णन प्राचल माध्यम में मौजूद प्रकीर्णन कणों के गुणों पर निर्भर करते हैं, जैसे कि उनका आकार, आकृति और सांद्रता। वर्तमान में, एक पंकिल माध्यम के विशेषता चिह्नित करने लिए, अर्थात्, माध्यम के प्रकीर्णन प्राचल को निर्धारित करने के लिए, कई तरीके मौजूद हैं, जिससे घटक कणों के विभिन्न भौतिक गुण प्राप्त किए जा सकते हैं। हालांकि, इस तरह के माध्यमों के विशेषताएं चिह्नित करने के लिए विवरण की गई अधिकांश विधियां या तो महंगी या जटिल हैं, जो किसी दिए गए अनुप्रयोग के लिए वांछित यथार्थता और मजबूती के अनुसार भिन्न होती हैं। इस थीसिस में, हम विश्लेषणात्मक और संख्यात्मक गणनाओं के संयोजन के साथ प्रयोगात्मक मापों का उपयोग करके पंकिल माध्यम से प्रकाश के प्रकीर्णन पर अपनी जांच प्रस्तुत करते हैं, इस लक्ष्य के साथ की वह तरीके अपेक्षाकृत सरल हो, कम घटकों की आवश्यकता रखती हो, और लागू करने में आसान होती हो।

हमारी कार्यप्रणाली में उचित रूप से रखे गए प्रकाश संसूचक का उपयोग करके एक पंकिल माध्यम में से आती हुई प्रकीर्ण रोशनी की माप करना शामिल है, और मापी गई शक्ति के साथ प्रकीर्णन प्राचल के विभिन्न संयोजनों के लिए संख्यात्मक रूप से प्राप्त प्रकीर्ण शक्ति की तुलना करना शामिल है। सिमुलेशनो को मॉटे

कार्लो विधि का उपयोग करके किया जाता है, और वह प्रकीर्णन प्राचल(ऐ) जिसके लिए संसूचक(ओ) पर प्रकीर्ण शक्ति मापी गई शक्ति के साथ मेल खाती है, उनको दिए गए पंकिल माध्यम के सटीक प्रकीर्णन प्राचल(ओ) के रूप में अनुमान लगाया जाता है। हमारे अध्ययन में, हम पद्धति को एक संसूचक पर दिए गए पंकिल माध्यम से बिखरे हुए प्रकाश को मापने के लिए लागू करते हैं, उस माध्यम के अनिसोट्रोपी प्राचल g के निर्धारण के लिए। प्रस्तावित विधि में, किसी दिए गए नमूने के अंतःक्रिया गुणांक μ_t को पहले बीयर-लैम्बर्ट नियम का उपयोग करके प्रकीर्णन हुआ प्रकाश के मापन से निर्धारित किया जाता है; फिर नमूने से किसी एक कोण पर प्रकीर्ण शक्ति को एक प्रकाश संसूचक का उपयोग करके मापा जाता है। मापी गई प्रकीर्ण शक्ति को शक्ति के अनुरूप माध्यम का g का अनुमान लगाया जाता है प्रकीर्ण शक्ति को शक्ति की g से संबंधित अंशांकन वक्र से, जो मोटे कार्लो सिमुलेशन से प्राप्त होता है। यह भी चर्चा की जाती है कि येही पद्धति लागू की जा सकती है गोलाकार कणों वाले मोनोडिस्पर्स पंकिल समाधानों के मामले में कण आकार प्राप्त करने के लिए। हालांकि, यह देखा जाता है कि संसूचक की एकल स्थिति के अनुरूप g (या कण आकार) के दो संभावित मान हैं। इसके बाद, हम दिखाते हैं कि प्रकीर्ण शक्ति को मापने के लिए दो अलग-अलग स्थानों पर रखे गए दो संसूचकों का उपयोग करके, g या कण आकार को विशिष्ट रूप से निर्धारित किया जा सकता है।

μ_t के अनुमान के लिए अविचलित संचरित प्रकाश की माप की आवश्यकता होती है, जिसके लिए संबंधित संसूचक को पंकिल नमूने से काफी दूर (≈ 1 मीटर) रखना होता है। इस आवश्यकता के कारण प्रायोगिक व्यवस्थाओं के थोक को कम करने के लिए, हम दिए गए नमूने से संचरित किरण को एकाधिक बार मोरने के हेतु समानांतर दर्पण की एक जोड़ी के उपयोग का भी प्रस्ताव करते हैं, किरण की प्रभावी पथ की लंबाई को बढ़ाने के लिए। यह संसूचक को नमूने के अपेक्षाकृत करीब रखकर μ_t का सटीक अनुमान लगाना संभव बनाता है, जिससे व्यवस्था सघन हो जाता है। हम और आगे सिमुलेशन के बजाय विश्लेषणात्मक गणनाओं का उपयोग करके एक पंकिल समाधान में सूक्ष्मवृत्त के आकार को निर्धारित करने के लिए एक विधि प्रस्तुत करते हैं, इस प्रतिबंध के साथ कि कण नमूने के अंदर एक बहुत छोटे क्षेत्र में केंद्रित हैं। इस विधि में नमूने के करीब रखे गए दो संसूचक की आवश्यकता होती है, अलग-अलग पदों में प्रकीर्ण शक्ति को मापने के लिए; प्रस्तावित योजना में, μ_t के अनुमान की बिल्कुल भी आवश्यकता नहीं है, जो फिर से एक सघन व्यवस्था की ओर ले जाता है।

मिश्रणों पर भी अध्ययन किया जाता है, जहां मिश्रण विभिन्न प्रकार के कणों से युक्त एक पंकिल माध्यम को संदर्भ करता है। मौलिक सिद्धांतों से, हम मॉन्टे कार्लो मॉडल का उपयोग करके मिश्रण में प्रकाश की प्रसार को सिमुलेट करने के लिए एक योजना पर पहुंचते हैं, और फिर इसे एक द्वि-फैलाव मिश्रण में स्थित ज्ञात प्रकार के घटकों की सांद्रता निर्धारित करने के लिए लागू करते हैं, पहले समान पद्धति का पालन करते हुए घटक कणों की विभिन्न सापेक्ष सांद्रता के लिए प्रकीर्ण शक्ति की मापी गई शक्ति से तुलना करके। अंत में, हम मॉन्टे कार्लो सिमुलेशन का उपयोग करके अलग-अलग परिचालन तरंग दैर्घ्य और संसूचक स्थितियों के लिए प्रकीर्ण शक्ति से संबंधित कण आकार या फिर g की अंशांकन वक्र को सिमुलेट करते हैं, और दिखाते हैं कि प्रायोगिक वयवस्था में इन भौतिक कारकों को उचित रूप से चुनकर हमारी पद्धति को डायनामिक रेंज और सेंसिटिविटी के संदर्भ में अनुकूलित किया जा सकता है। हम और आगे दिखाते हैं कि प्रयोगात्मक वयवस्था को ऑप्टिकल फाइबर के द्वारा नमूने से/तक प्रकाश की परिवहन करके लागू किया जा सकता है, जो मजबूती, स्थायित्व और रिमोट सेंसिंग अनुप्रयोगों के लिए टेलीमेट्री के दायरे जैसे अतिरिक्त लाभ प्रदान करता है।

Contents

Certificate	i
Acknowledgements	iii
Abstract	v
Contents	ix
List of Figures	xiii
List of Tables	xxiii
1 Introduction	1
1.1 Introduction	1
1.2 Motivation and objectives of the thesis	8
1.3 Organization of the thesis	9
2 Scattering Theory and Monte Carlo Modelling of Light Propagation inside a Turbid Medium	15
2.1 Scattering Theory	15
2.1.1 Scattering matrix	15
2.1.2 Cross sections and phase function	18
2.1.3 Special cases: Mie theory and Rayleigh theory	19
2.2 Monte Carlo Modelling of Light Propagation inside a Turbid Medium	21
2.2.1 Photon packets: Definition	21
2.2.2 Propagation of photon packets inside the turbid medium	22
2.2.3 Sampling of variables: Inverse distribution method	24

2.2.4	Determination of the step size s	24
2.2.5	Determination of scattering angle θ and azimuthal angle ϕ	26
2.2.6	Choice of phase function	27
2.2.7	Accounting for absorption	29
2.2.8	Discussion	29
2.3	Summary	30
3	Method to Determine the Anisotropy Parameter of a Turbid Medium	31
3.1	Introduction	31
3.2	Methodology	34
3.2.1	Experimental setup	34
3.2.2	Determination of interaction coefficient μ_t	35
3.2.3	Estimation of anisotropy parameter g	36
3.2.4	Monte Carlo simulation of the experimental setup	37
3.2.5	Preparation of turbid samples	38
3.3	Results and Discussion	39
3.4	Summary	45
4	Determination of the Size of Microspheres in Monodisperse Turbid Solutions	47
4.1	Introduction	47
4.2	Methodology	49
4.2.1	Experimental setup	49
4.2.2	Relative measurements to determine particle size	51
4.2.3	Normalization with reference sample	52
4.2.4	Measurements at different concentrations	53
4.3	Results and Discussion	53
4.4	Summary	56
5	Compact Setup to Determine Size and Concentration of Spherical Particles in a Turbid Medium	59
5.1	Introduction	59

5.2	Methodology	61
5.2.1	Angle-selective filter for transmitted light	61
5.2.2	Experimental setup	63
5.2.3	Determination of particle size and concentration	66
5.3	Results and Discussion	68
5.4	Summary	72
6	Method to Determine the Concentrations of Constituents in a Bidisperse Turbid Medium	75
6.1	Introduction	75
6.2	Monte Carlo Model for Light Scattering in Turbid Mixtures	78
6.3	Methodology	83
6.3.1	Experimental setup	83
6.3.2	Preparation of samples	84
6.3.3	Determination of constituent concentrations	86
6.4	Results and Discussion	88
6.4.1	Interaction coefficient of bidisperse mixtures	88
6.4.2	Constituent concentrations of bidisperse mixtures	89
6.5	Determination of Anisotropy Parameter g of a Turbid Medium using Mixtures .	93
6.6	Summary	95
7	Design Considerations for Scattered Light Measurements using Optical Fibers	97
7.1	Introduction	97
7.2	Influence of Wavelength and Detector Position	99
7.2.1	Scattered power vs particle size	100
7.2.2	Scattered power vs anisotropy parameter g	102
7.3	Integration with Optical Fibers	104
7.3.1	Determination of interaction coefficient μ_t	105
7.3.2	Simulation of scattered power: Influence of numerical aperture	106
7.4	Further Design Issues	109

7.5 Summary	110
8 Summary and Scope for Future Work	111
Appendix A Determination of Scattering Angle	115
Appendix B Vertical Displacement of the Scattered Beam	117
References	121
List of Publications	141
Author's Biography	143

List of Figures

2.1	(a) A plane polarized wave is incident on a particle, and a wave scattered at angle θ is shown. Since the scattering is elastic, the wavelength of the scattered light is the same as that of the incident light, but the propagation vectors \vec{k}_i and \vec{k}_s are in different directions. (b) Waves scattered at angle θ form a cone around the z-axis, which is fixed to be the direction of the incident light. Thus, the azimuthal angle ϕ , which is the angle between the x-axis and the projection of the scattered wave on the x-y plane, is required in addition to θ in order to determine the direction of the scattered wave uniquely. Here, the straight arrows represent the propagation vectors (the wavefronts are not shown); the origin corresponds to the position of the scattering particle.	16
2.2	The total energy of the scattered wave from a scattering particle depends on C_s , with the amount of light scattered in each direction described by the phase function $p(\theta, \phi)$. By treating the incident light energy as a collection of energy packets or photon packets, an equivalent stochastic picture is obtained in which several packets are incident on the particle, some of which undergo scattering in different directions.	22

2.3	(a) Propagation of photon packets inside a turbid medium. Here propagation of three packets are shown, one of which reaches the detector. All three packets have the same step size till the first point of scattering, whereas the subsequent step sizes are different. Note that this is a specific example to illustrate the stochastic nature of the process; the first scattering event may as well be at different positions for different photon packets. (b) Scattering angle θ_q and step size s_q after the q^{th} interaction event. The azimuthal angle ϕ (not shown) is also incorporated if the model is three dimensional.	23
2.4	A photon packet propagates through a distance s_1 in the turbid medium. A segment of length ds' is considered, located at distance s' from the origin of the packet. From the relevant probability distributions, the step size is obtained in terms of μ_t and ξ	25
3.1	Schematic of the experimental setup to measure the scattered light and the undeviated transmitted light from a turbid sample, at detectors D_1 and D_2 , respectively. The scattered power at D_1 depends on the scattering parameters of the medium, and the measurement at D_2 is used to determine the interaction coefficient μ_t	35
3.2	Measurement of ‘unscattered’ light I to determine the interaction coefficient μ_t of a turbid sample; I_0 is the incident light and L is the interaction length. In practice, the forward scattered light and a small amount of light scattered at extremely small angles always reach the detector, but their contribution is negligible if the detector is placed at a large distance from the turbid sample. . . .	36
3.3	Schematic representation of propagation of a photon packet through a turbid medium, where a packet which reaches the detector has been shown. The effect of energy loss and deviation of the packet due to refraction at the cuvette wall is also incorporated in the simulation.	37

3.4	Variation of anisotropy parameter g and scattering cross section C_s with particle size (diameter) for a polystyrene sphere suspended in water, corresponding to wavelength $\lambda_0 = 632.8$ nm. The calculations have been performed using the <i>MiePlot</i> software by Philip Laven [Laven, n.d.]. The particle diameters range from 50 nm to 1000 nm in steps of 50 nm. Since polystyrene is non-absorbing at λ_0 , $C_s = C_t$, the total cross section, in this case.	39
3.5	Measurement of the scattered light from the turbid sample at off-axis detector D_1 , whose position is described in terms of the longitudinal separation $l_z = 12$ cm and the off-axis displacement $l_x = 7$ cm. The top view is shown, which means the page is parallel to the table on top of which the experimental setup (Fig. 3.1) is situated.	40
3.6	The a) Mie phase function and the b) Henyey-Greenstein (HG) phase function for the four sizes of polystyrene spheres used to prepare the turbid samples for the experiment. The scattering angle ranges from 0° to 180° in steps of 0.05° . The anisotropy parameter g corresponding to each particle size has been calculated using the Mie phase function.	41
3.7	Calibration curves obtained from Monte Carlo simulations for interaction coefficients 0.1, 0.2 and 0.3 cm^{-1} , by using a) Henyey-Greenstein phase function, and b) Mie phase function. The markers correspond to the experimental data, and error bars are also shown. It can be seen that the difference between the simulated scattered powers and the measured scattered powers is much less for the case of the Mie phase function in comparison to the Henyey-Greenstein phase function.	44

4.1	Measurement of the scattered light from spherical particles in the turbid sample at an off-axis detector. The particles are suspended at the midpoint of the cuvette. The scattering angle is θ_e and can be assumed to be the same for all particles since the area of the detector is small. The total path length travelled by the light before reaching the detector is r_e (not labelled).	50
4.2	Experimental setup to measure the scattered light from the spherical particles at two detectors, D_1 and D_2 , corresponding to the scattering angles θ_1 and θ_2 . The positions of the two respective detectors are defined in terms of (x_1, z_1) and (x_2, z_2)	51
4.3	Ratio of the Mie phase function vs. particle size (diameter) for various pairs of scattering angles. The Mie phase function corresponding to different particles sizes was calculated using <i>MiePlot</i> [Laven, n.d.]. The particle size was changed in steps of 50 nm to obtain the curves. These calibration curves can be used to determine the particle size from the experimentally determined ratio of phase function.	52
4.4	Scattered power at detector D_1 vs. that at D_2 for different concentrations of particles with sizes a) 600 nm and b) 3000 nm. The slopes of the straight line fits are the values of M_{exp} for the respective particle sizes; the intercept is due to background noise and of no use in our methodology.	54
4.5	Calibration curves relating the ratio of phase function to the particle size, for two different configurations of the detectors corresponding to a) $\theta_1 = 11.2^\circ$ and $\theta_2 = 20.5^\circ$, and b) $\theta_1 = 8.75^\circ$ and $\theta_2 = 21.95^\circ$. The phase functions have been calculated from Mie theory, using the <i>MiePlot</i> software [Laven, n.d.]. For both curves, the experimentally obtained ratios of phase function are shown with markers, which are transparent in order to show the error bars as well. The green marker corresponds to the reference sample of particle size 800 nm, which is used to determine the ratio of phase function for the other sizes [Eq. (4.10)].	55

5.1	Measurement of the scattered light at a detector with aperture a , which is a) placed at a large distance from the turbid sample, and b) placed near the sample, but the effective path length is large due to successive reflections of the transmitted light at two parallel mirrors. The detector is placed symmetrically with respect to the direction of the unscattered light beam. The various geometrical factors determine the angular selectivity of the aperture in both cases.	62
5.2	Experimental setup to measure the scattered light at two angular positions by the detectors D_1 and D_2 . The undeviated transmitted light is measured at detector D_3 , and the path length of the transmitted beam is effectively increased due to the pair of parallel mirrors. A beam splitter is used to measure a part of the transmitted light at detector D_4 , placed far from the sample in the conventional configuration, in order to verify the results.	64
5.3	A compact configuration based on the experimental setup shown in Fig. 5.2. Detectors D_1 and D_2 are used to measure the scattered light at two different angular positions. The size of this compact setup is approximately 20 cm×20 cm, because detector D_3 is now placed close to the sample, while the transmitted beam travels a large effective path length due to repeated reflections from the pair of parallel mirrors.	66
5.4	The Mie phase function for the two sizes of polystyrene spheres present in the turbid samples for the experiment. The scattering angle ranges from 0° to 180° in steps of 0.05°	67

5.5	Comparison of the estimated values of μ_t from measurements at the two detectors D_3 and D_4 , which are placed near and far from the sample, respectively (see Fig. 5.2). The blue circular markers and the green square markers correspond to samples comprising particles of sizes 600 nm and 2000 nm, respectively. The dotted line corresponds to $y = x$, and the error bars are also shown.	68
5.6	Simulated scattered power for a turbid medium with $\mu_t = 0.173 \text{ cm}^{-1}$ and particle size = 2000 nm, at detectors D_1 and D_2 . The particle size was changed in steps of 100 nm and 10 million photon packets were simulated for each particle size. The experimentally obtained power at a particular detector may correspond to the simulated power for more than one particle size, but only one particle size corresponds to the measured power levels at both the detectors.	70
5.7	Simulated scattered power for the same medium as shown in Fig. 5.6; the particle size is changed in steps of 10 nm and 100 million photon packets are simulated for each particle size. The left and the right axes represent the powers at detectors D_1 and D_2 , respectively. The measured scattered powers corresponding to the respective simulated powers give us the correct size of the particles suspended in the turbid medium.	70
6.1	a) A photon packet travelling a distance s_1 in a turbid mixture of volume $V = LA$, which comprises multiple types of suspended particles. b) The distance $s_1 = z_1/\mu_z$ is divided into m equal segments of length Δz and volume ΔV . c) Shaded cylindrical volume in which a particle must be present to scatter the photon packet in that particular segment.	79
6.2	Experimental setup to measure the scattered power at an off-axis detector, D_1 , and to estimate μ_t by measuring the undeviated transmitted light at detector D_2 . The setup is similar to the one shown in Figs. 3.1 and 3.5, but the geometrical parameters are slightly different since the detector is placed arbitrarily.	84

6.3	Two monodisperse turbid solutions A and B with respective volumes V_1 and V_2 , which comprise two different types of particles, are mixed together to form a bidisperse mixture. n_{m1} and n_{m2} are the concentrations, and N_1 and N_2 are the total number of particles, in samples A and B, respectively.	85
6.4	Flowchart for Monte Carlo simulation of the experimental setup, to obtain the fractional scattered power from the bidisperse mixture.	87
6.5	Reference plots of the fractional scattered power vs p_{1s} for two bidisperse mixtures A and B (comprising polystyrene spheres), obtained from Monte Carlo simulations. It can be seen that the variation is monotonic, i.e., there is one-to-one correspondence between p_{1s} and the scattered power. The estimated value of p_{1s} corresponding to the measured scattered power is shown by dotted lines for both the mixtures. Error bars are not shown because the variation in the scattered powers are negligible compared to the scale.	90
6.6	Variation of the fractional scattered power collected at the off-axis detector with the anisotropy parameter g of the known solution in the mixture, when the unknown sample has anisotropy parameter g' equal to (a) 0.7 and (b) 0.5, for different values of p_{1s} . These curves have been obtained using the Monte Carlo model for mixtures discussed earlier in the chapter, and the interaction coefficient μ_t has been kept fixed at 0.1 cm^{-1} in the simulations. The curves intersect at the point where the anisotropy parameter of the known sample is equal to g' . In the actual method which is being proposed, the calibration curves will be obtained experimentally, and no simulations would be required.	94
7.1	Measurement of scattered light from a turbid medium at an off-axis detector. The particles in the turbid medium are polystyrene spheres; the medium is semi-infinite and the interaction length is equal to 1 cm.	99

7.2	Simulated calibration curves relating the fractional scattered power to the particle size for different values of off-axis displacement l and wavelength λ . The particle size has been varied in steps of 50 nm.	101
7.3	The curves in Fig. 7.2 are shown separately to emphasize the variation of the scattered power with l and λ . Figures a), b), and c) show the variation of the curves with l for different wavelengths, and figures d), e) and f) show the variation with λ for different values of l	101
7.4	Variation of anisotropy parameter g with particle size (diameter) for polystyrene spheres suspended in water, corresponding to different wavelengths. The particle size has been varied in steps of 50 nm. The calculations have been performed using the <i>MiePlot</i> software by Philip Laven [Laven, n.d.].	102
7.5	Simulated calibration curves relating the fractional scattered power to the anisotropy parameter g for different values of off-axis displacement l and wavelength λ . g has been varied corresponding to the variation of the particle size in steps of 50 nm.	102
7.6	Variation of size parameter χ with anisotropy parameter g for different wavelengths. It can be seen that the value of χ corresponding to a particular value of g does not depend on wavelength.	103
7.7	Mie phase function corresponding to the three sizes of polystyrene sphere particles at the different wavelengths listed in Table 7.2.	103
7.8	A setup integrated with optical fibers used to measure the undeviated transmitted– and the scattered light from a turbid medium. The proposed setup is compact due to the use of components such as the laser diode and a pair of parallel mirrors.	104

7.9	Measurement of the undeviated transmitted light from a turbid medium using optical fibers. Light from a He-Ne laser is coupled into the input fiber using a microscope objective (MO), and the output (light) of the fiber is collimated using another MO, which is then incident on the turbid sample. The undeviated transmitted light from the turbid sample is multi-folded at a pair of parallel mirrors to increase the effective path length ($L_M = 113$ cm in our case). A convex lens (focal length 60 mm) is used to focus the undeviated transmitted light into another fiber which carries the light to detector D_1 . The measurements are also performed in the conventional bulk configuration at detector D_2 , placed far from the sample (total path length $L = 115.5$ cm), in order to verify the results.	105
7.10	Estimated values of μ_t from the measurements at detectors D_1 and D_2 , which correspond to the optical fiber-based configuration and the conventional configuration of the setup, respectively. The values match within the limits of experimental error.	106
7.11	Calibration curves relating the scattered power to particle size for different values of wavelength λ , off-axis displacement l , and numerical aperture NA of the collecting fiber. It can be seen that the dependance on λ and l is the same as was seen in Fig. 7.2, with an additional dependence on NA. Multiple values of NA in a label signifies that the same curve was obtained for different values of NA.	107
7.12	Dependance of the calibration curve on numerical aperture (NA) for different combinations of λ and l . The label of each curve denotes the corresponding value of NA used to obtain the curve. It can be seen that there exists a cut-off value of numerical aperture, NA_c , below which the scattered power decreases.	108
7.13	Maximum angle subtended by a singly scattered photon packet at the collecting fiber. The maximum angle is $\theta_0 = \tan^{-1}(l/4)$, from which $NA_0 = \sin \theta_0$ can be calculated.	109

A.1	Determination of scattering angle θ_e corresponding to the detector position (x, z) .	115
B.1	A schematic of the angle-selective optical filter based on a pair of mirrors for multi-folding the laser beam (see Fig. 5.1).	118
B.2	Determination of the lengths TD and PQ from geometry (Expanded view of $\Delta\alpha$ at the input and exit planes of the mirror pair).	118

List of Tables

3.1	Comparison of the experimentally obtained scattered power P_{exp} and the simulated scattered powers P_{Mie} and P_{HG} for the Mie phase function and the Henyey-Greenstein phase function, respectively, corresponding to their respective optimized configurations of the setup. The results for all the samples, i.e., a combination of four particle sizes and three values of μ_t , are shown. It can be seen that the Mie phase function gives more accurate results than the Henyey-Greenstein phase function, which is expected since the particles are spherical.	43
4.1	The size of particles obtained from the calibration curve, corresponding to the calculated values of the ratio of the phase function, for the various samples. The results for two different configurations of the detectors are shown in the tables (a) and (b). The sample with size 800 nm is used as the reference sample (RS). The actual microsphere sizes for the samples are also shown for comparison. In case of the second configuration, the size for the samples with actual particle size 500 nm could not be estimated because the calibration curve was almost flat, leading to higher error.	56
5.1	Comparison of the estimated values of μ_t from measurements at the two detectors D_3 and D_4 for particles of two different diameters. The range of values match within expectations, and thus the use of the pair of parallel mirrors allows us to accurately measure the undeviated transmitted light while keeping the detector close to the sample.	69

- 5.2 Estimated particle size and concentration (n) for different turbid samples. The small difference between the sizes obtained using D_1 and D_2 is due to experimental errors, and the average of the two values is taken to be the correct particle size. For calculation of n , the cross sections for the two sizes were $C_{t, 600 \text{ nm}} = 3.04 \times 10^{-9} \text{ cm}^2$ and $C_{t, 2000 \text{ nm}} = 1.02 \times 10^{-7} \text{ cm}^2$ 71
- 6.1 Experimentally determined interaction coefficients of monodisperse samples and their mixtures with varying concentration of particles. The monodisperse samples were prepared using polystyrene particles of sizes 500 nm and 2 μm , respectively, and their interaction coefficients are μ_{t1} and μ_{t2} . The estimated interaction coefficients of the bidisperse mixtures are referred to as simply μ_t . The values of $(\mu_{t1} + \mu_{t2})$ and μ_t match closely, as expected from Eq. (6.1). . . . 88
- 6.2 Estimated values of p_{1s} , along with the calculated constituent concentrations, n_1 and n_2 , for bidisperse turbid mixtures comprising particles of sizes 2 μm and 3 μm . The actual values of p_{1s} , n_1 , and n_2 of the prepared samples are given in parentheses, with respect to which the relative errors are calculated. For calculation of concentrations n_1 and n_2 , the cross sections for the two sizes were $C_{t, 2 \mu\text{m}} = 1.02 \times 10^{-7} \text{ cm}^2$ and $C_{t, 3 \mu\text{m}} = 1.21 \times 10^{-7} \text{ cm}^2$. The parameters corresponding to the turbid mixture A in Fig. 6.5 are shown in bold. 91
- 6.3 Estimated values of p_{1s} , along with the calculated constituent concentrations, n_1 and n_2 , for bidisperse turbid mixtures comprising particles of sizes 1 μm and 3 μm . The actual values of p_{1s} , n_1 , and n_2 of the prepared samples are given in parentheses, with respect to which the relative errors are calculated. For calculation of concentrations n_1 and n_2 , the cross sections for the two sizes were $C_{t, 1 \mu\text{m}} = 1.99 \times 10^{-8} \text{ cm}^2$ and $C_{t, 3 \mu\text{m}} = 1.21 \times 10^{-7} \text{ cm}^2$. The parameters corresponding to the turbid mixture B in Fig. 6.5 are shown in bold. 92

7.1	Refractive indices of polystyrene particles, n_p [Sultanova et al., 2009], distilled water, n_m [Hale and Querry, 1973], and quartz, n_g [Tan, 1998], corresponding to the three wavelengths (λ) used in the simulations.	100
7.2	Three different particle sizes (diameters) corresponding to three different wavelengths, chosen such that they have similar values of n_r , χ , and g . Note that n_r depends on the wavelength but not on the particle size; it has been listed in the table after the particle size only for ease of comparison.	103
7.3	Calculated values of NA_0 from geometry (Fig. 7.13) vs the cut-off value NA_c obtained from Monte Carlo simulations, for different values of off-axis displacement l . It can be seen that the values match closely, which confirms that the existence of the cut-off is due to the dominance of single scattered photon packets incident on the collecting fiber.	109

